Self-Consistent Reaction Field Calculations of Aqueous Al^{3+}, Fe^{3+}, and Si^{4+}: Calculated Aqueous-Phase Deprotonation Energies Correlated with Experimental $\ln(K_a)$ and pK_a

J. D. Kubicki*

Department of Geosciences, The Pennsylvania State University, University Park, Pennsylvania 16802

Received: May 10, 2001; In Final Form: July 9, 2001

Reaction energies for the deprotonation of $Al^{3+}\cdot 6(H_2O)$, $Fe^{3+}\cdot 6(H_2O)$, and $Si(OH)_4$ were calculated using Hartree−Fock and density functional methods with 6-311+G(d,p) (for Al^{3+} and Si^{4+}) and 6-311G(d) (for Fe^{3+}) basis sets. Theoretical energies were calculated using a supermolecule approach (i.e., explicit hydration of the solute) combined with the Integral Equation Formalism Polarized Continuum Model (IEFPCM; Cancès et al., 1997, *J. Chem. Phys*. **107**, 3032) and the Self-Consistent Isodensity Polarized Continuum Model (SCIPCM; Keith and Frisch, 1994, *ACS Symp. Ser*. **56**, 22) in Gaussian 98. Tests on the effects of increasing the number of water molecules explicitly included in the supermolecule were also carried out. Additional water molecules in the energy minimizations of $Al(OH)_3$, $Fe(OH)_3$, and $[Si(OH)_3(OH_2)]^+$ resulted in 5-coordinate complexes for all three species. Correlations of deprotonation energies with observed $\ln(K_a)$ values are good for individual cations. These correlations suggest that the combined supermolecule/continuum approach can give reliable pK_a estimates, provided that the structural optimization reflects the aqueous-phase solute and that the basis set includes polarization and diffuse functions. An estimate is made of the pK_a of the reaction—$[Si(OH)_3(OH_2)]^+_{(aq)} \leftrightarrow Si(OH)_{4(aq)} + H^+_{(aq)}$—which has not yet been measured. A value of $pK_a \approx -2$ is predicted in this study.

Introduction

Correlation of deprotonation energies vs experimental pK_a [$pK_a = -\log(K_a) = -2.303\ \ln(K_a)$] values have a thermodynamic basis in the following equations

$$\ln(K_a) = -(\Delta G/RT) \tag{1}$$

$$RT\ln(K_a) = -\Delta G = -\Delta H + T\Delta S \tag{2}$$

$$RT\ln(K_a) - T\Delta S = -\Delta H \tag{3}$$

A plot of $\ln(K_a)$ vs $-\Delta H$ should have a slope equal to RT and an intercept equal to $-T\Delta S$ provided that the ΔS term is relatively constant for each hydrolysis reaction. This is a major assumption in this approach. Actual variation in the ΔS of hydrolysis reactions may be significant because the pH range over which hydrolysis occurs can be wide. Hence, changes in the long-range structure of water over this pH range may influence the ΔS of removing a proton from the metal solvation sphere and creating a H_3O^+ (or alternatively an H_2O under basic pH conditions). This source of error could be investigated in the future using larger scale calculations with hybrid quantum mechanics/molecular mechanics approaches such as ONIOM.[1]

The T predicted in this correlation should correspond to the experimental temperature under which the $\ln(K_a)$ were determined. In this case, experiments were conducted at 25 °C or 298 K. Although energy minimizations are performed athermally (i.e., 0 K), force constant analyses were performed with a $T = 298.15$ K; hence, the energies of these models should correspond to experimental systems when the thermal correction to the energy is included in addition to the zero-point energy.

The ΔH term is approximated by the calculated $\Delta E_{(aq)}$ in these model calculations. The difference between the two is the PV term included in the enthalpy, and this term is small compared to ΔH or ΔE at ambient conditions. Using the above equation, it is not necessary to include an experimental ΔS with a theoretical ΔH in order to predict a ΔG and a pK_a. This approach makes the method self-consistent, and the separate prediction of T and ΔS for the system can be used to test the validity of the model calculations when these values are available from experiment.

A computational method for predicting pK_as of inorganic aqueous species is being developed for a number of purposes.[2−5] First, modeling the acid−base behavior of complexes that have known pK_as is a useful goal. If methods for predicting pK_as can be calibrated on known systems, then it should be possible to predict pK_as for complexes that are more difficult to measure. Second, we would also like to model complexation reactions among species that lead to precipitation of oxides and oxyhydroxides. Obtaining an accurate theoretical description of these components in solution is a first step toward modeling complexation and nucleation. Third, complexation reactions between aqueous inorganic species and organic ligands are important in the environment.[6] Accurate prediction of the pK_as for both the inorganic and organic parts of these reactions is necessary before these complexation reactions can be modeled as a function of solution pH. Fourth, prediction of the individual pK_as for mineral surface sites can be used to understand adsorption reactions. Electrostatic forces at the mineral−water interface spread out the distribution of pK_as from individual sites, making the pK_as indistinguishable, so that potentiometric studies detect only one or two "mineral surface" pK_as. The pK_as for numerous surface sites may vary significantly, however, from bulk mineral surface pK_as. We are particularly interested in defect sites that may be highly reactive.[7] Some adsorption sites may occur in low

* To whom correspondence should be addressed. Phone: (814) 865-3951. Fax: (814) 863−8724. E-mail: kubicki@geosc.psu.edu.

10.1021/jp011793u CCC: $20.00
Published on Web 08/16/2001

concentrations[8] and may be undetected in potentiometric experiments. Hence, with this work, an attempt is made to develop a method that can predict intrinsic pK_as for mineral surface species as well as aqueous species.

Methods

Energy minimizations were performed with HF/3-21G(d,p) basis sets[9,10] within Gaussian 98[11] using internal redundant coordinates.[12] Zero-point (ZPE) and thermal energies were also derived from force constant analyses using the HF/3-21G(d,p) basis sets. ZPEs were corrected by 0.941[13] to compensate for errors induced by the Hartree−Fock approximation, the limited basis set, and anharmonic effects.[14] For Fe^{3+}, structures were re-optimized with hybrid molecular orbital/density functional calculations using the Becke exchange functional[15] and the Lee−Yang−Parr correlation functional[16] with a 6-311G(d) basis set because this method has been shown to provide reliable structures for aqueous Fe^{3+}.[17] A scale factor of 0.980 was used for these B3LYP/6-311G(d) ZPEs.[13] Up to nineteen water molecules were used to hydrate the model solutes. Model aqueous-phase energies were calculated using these optimized structures and HF/6-311+G(d,p) and B3LYP/6-311G(d) basis sets within the Integral Equation Formalism Polarized Continuum Model (IEFPCM)[18] and Self-Consistent Isodensity Polarized Continuum Model (SCIPCM)[19] without further energy minimization.

Calculated aqueous deprotonation reaction energy changes, $\Delta E_{(aq)}$, such as

$$M^{3+}\cdot 6(H_2O) \leftrightarrow M(OH)^{2+}\cdot 5(H_2O) + H^+ \qquad (4)$$

(where $M^{3+} = Al^{3+}$ or Fe^{3+}) were balanced by the model reaction

$$H_2O\cdot 8(H_2O) + H^+ \leftrightarrow H_3O^+\cdot 8(H_2O) \qquad (5)$$

The reactions $Si(OH)_4 \leftrightarrow [SiO(OH)_3]^- + H^+$ and $[SiO(OH)_3]^- \leftrightarrow [SiO_2(OH)_2]^{2-} + H^+$ were balanced with

$$OH^-\cdot 8(H_2O) + H^+ \leftrightarrow H_2O\cdot 8(H_2O) \qquad (6)$$

because these reactions occur above pH 7 where reaction 6 is likely to be dominant. Use of this scheme provides a self-consistent prediction of the deprotonation energies for all species.

Results and Discussion

Al^{3+} Hydrolysis. Structural changes upon deprotonation of $Al^{3+}\cdot 6(H_2O)$ predicted with HF/3-21G(d,p) basis sets have been described previously.[20,21] Energy minimizations with B3LYP/6-31G(d) and MP2/6-311+G(d,p) did not change the bond lengths by more than a few percent. All three methods result in calculated bond lengths that agree to within 0.04 Å of those obtained from X-ray diffraction.[22] It is interesting to note that the HF/3-21G(d,p) basis set predicts Al−(OH_2) bond lengths closest to experiment in this case (1.91 Å calculated vs 1.88 to 1.90 Å experimental). In addition, the $Al^{3+}\cdot 6(H_2O)$ calculated structure is similar to that obtained using ab initio molecular dynamics simulations.[23] Removal of the first two protons does not change the coordination state of the complex, but the shortening of the deprotonated Al−(OH) bonds causes the remaining Al−OH_2 bonds to lengthen. These results are consistent with the observation of increasing H_2O exchange rates with Al^{3+} in aqueous solutions using NMR spectroscopy.[24]

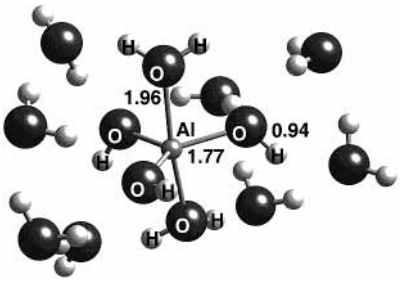

Figure 1. Five-fold coordinate aqueous Al^{3+} model of $[Al(OH)_3(H_2O)_2]\cdot 8(H_2O)$ as calculated with HF/3-21G(d,p) basis set in Gaussian 98.[11] Average bond lengths are given in Å. In all figures, the shorter of the two M−O bond lengths corresponds to the M-OH bond and the longer corresponds to the M-OH_2 bond. For clarity, all atoms within the primary coordination sphere have been labeled wherever possible when a second solvation shell has been modeled.

Upon removal of the third proton from this species, a tetrahedral configuration becomes more stable in the energy minimization. This configuration, however, is an artifact of the cluster approximation caused by including only two water molecules of solvation. Energy minimization of the molecular cluster $[Al(OH)_3]\cdot 9(H_2O)$ produces a 5-fold coordinate Al species, $[Al(OH)_3(H_2O)_2]\cdot 7(H_2O)$, where two of the H_2O molecules are bonded directly to the Al^{3+} cation (Figure 1). Note that the two axial H_2O molecules are much more weakly bonded to the Al^{3+} (1.96 Å) compared to the equatorial OH^- groups (1.77 Å). There is even a significant difference between the Al−O bond lengths of the two axial H_2O molecules. The fifth bond, which was not present in the under solvated complex, is longer (1.99 Å) than the axial bond present in $[Al(OH)_3(H_2O)]\cdot 2(H_2O)$ (1.99 Å vs 1.94 Å).

Addition of a solvation sphere around the $[Al(OH)_4]^-$ complex to form $[Al(OH)_4]^-\cdot 9(H_2O)$ does not affect the coordination state. The Al^{3+} remains tetrahedral as is observed in aqueous solutions above pH 5.[25] Similarly, a second solvation sphere around the $Al^{3+}\cdot 6(H_2O)$ complex to form $Al^{3+}\cdot 19(H_2O)$ does not change the coordination state. Only minor (~2%) changes in the bond distances were calculated between the $Al^{3+}\cdot 6(H_2O)$ and the $Al^{3+}\cdot 19(H_2O)$ clusters,[21] which is consistent with another recent study.[26] Consequently, an accurate description of solvation may be most critical for 5-coordinate species.

Using the structures predicted for the Al^{3+} hydrolysis series with HF/3-21G(d,p) basis sets and a single solvation sphere around the Al^{3+} cation, molecular energies for each complex in aqueous solution were calculated with HF/6-311+G(d,p) basis sets and IEFPCM solvation.[18] The energy differences between the $Al^{3+}\cdot 6(H_2O)$ complex and the deprotonated species were balanced by the energy of proton solvation [reaction 5] to obtain $\Delta E_{(aq)}$. Figure 2 shows the correlation of the calculated $-\Delta E_{(aq)}$ with experimental $\ln(K_a)$ values.[27] The linear correlation is good ($R^2 = 0.93$). The slope of this line should be equal to RT [eq 3], and the calculated temperature from the slope of this line is equal to 326 K. The calculated value is close to 298 K considering the approximations made here. Furthermore, significant improvement over the 475 K previously calculated[21] has been achieved even though this work excludes the cavitation correction term.[13] The slope calculated in this manner is much closer to the correct value than similar plots using the same basis set and gas-phase deprotonation energies that can result in calculated temperatures of 1000 K (unpublished results). However, the ΔS value calculated from the intercept of Figure 2 (eq 3) is equal to 316 J/mol-K. This value is large compared to experimentally derived entropy changes for aqueous deprotonation reactions of approximately 100 J/mol-K.[28] On the basis

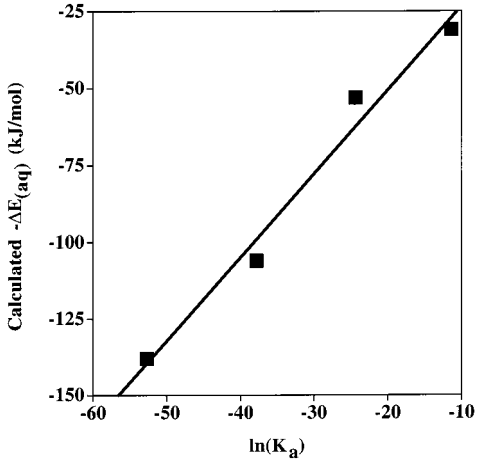

Figure 2. Calculated Al^{3+} hydrolysis deprotonation energies plotted against experimental ln(K_a) (ref 27).

of the good $\Delta E - \ln(K_a)$ correlation and the fact that calculated ^{27}Al NMR chemical shifts of these Al^{3+} complexes match experimentally observed values,[21,29] it appears that these models represent reasonable configurations of Al^{3+} species in aqueous solutions. Improvements (i.e., increasing explicit solvation, basis set size and level of electron correlation, and performing energy minimizations within the polarized continuum) could be made in the calculations that could produce better thermodynamic values.

Fe^{3+} Hydrolysis. Structures in the Al hydrolysis series were calculated with HF/3-21G(d,p) basis sets because this level of theory has been an efficient method for predicting structures, frequencies and NMR chemical shifts of aluminum species.[21,29] Although the Fe^{3+} hydrolysis series is similar to that of Al^{3+} in aqueous solution,[6] the presence of partially filled d-orbitals and unpaired spins on Fe^{3+} could cause significant errors when using the Hartree−Fock approximation.[17] Consequently, the Fe^{3+} hydrolysis series was calculated using the corresponding energy minimized structures computed for the Al hydrolysis series as starting configurations. The Fe^{3+} complexes were then optimized with the HF/3-21G(d,p) basis set. Minimum energy structures obtained at this lower level of theory were then re-optimized with the B3LYP/6-311G(d) method (Figure 3), which should be more reliable for Fe^{3+}-species.[17]

Model Fe−OH_2 bond lengths in [Fe^{3+}·6(H_2O)] were 2.03 and 2.04 Å for each method compared to an experimental range of 1.99−2.06 Å.[30] Table 1 shows a comparison of the bond lengths and HOH angles of the H_2O molecules bonded to Fe^{3+} as calculated with the two methods for species within the hydrolysis series. In general, the two methods result in similar structures. B3LYP/6-311G(d) bond lengths are a few percent longer and the bond angles a few percent smaller than the HF/3-21G(d,p) structures. The main difference is that the HF/3-21G(d,p) calculation predicts an octahedral [$Fe(OH)_2(H_2O)_4$]$^+$ complex and the B3LYP/6-311G(d) calculation results in a pentacoordinate [$Fe(OH)_2(H_2O)_3$]$^+$·(H_2O) complex (Figure 3c). Hence, although the HF/3-21G(d,p) method produces reasonable estimates of structure for these complexes, the energies of the Fe^{3+} hydrolysis series will be calculated based on the B3LYP/6-311G(d) structures in this paper.

Configurations of the complexes Fe^{3+}·6(H_2O) through [$Fe(OH)_4$]$^-$·2(H_2O) calculated with B3LYP/6-311G(d) are illustrated in Figure 3. The structures in Figure 3a-c are close to minimum energy structures calculated earlier[2] for these species using B3LYP/6-311G(d) on the Fe^{3+} and B3LYP/6-31G(d) for the ligands (H_2O and OH^-). We note that the [$Fe(OH)_4$]$^-$·2(H_2O)

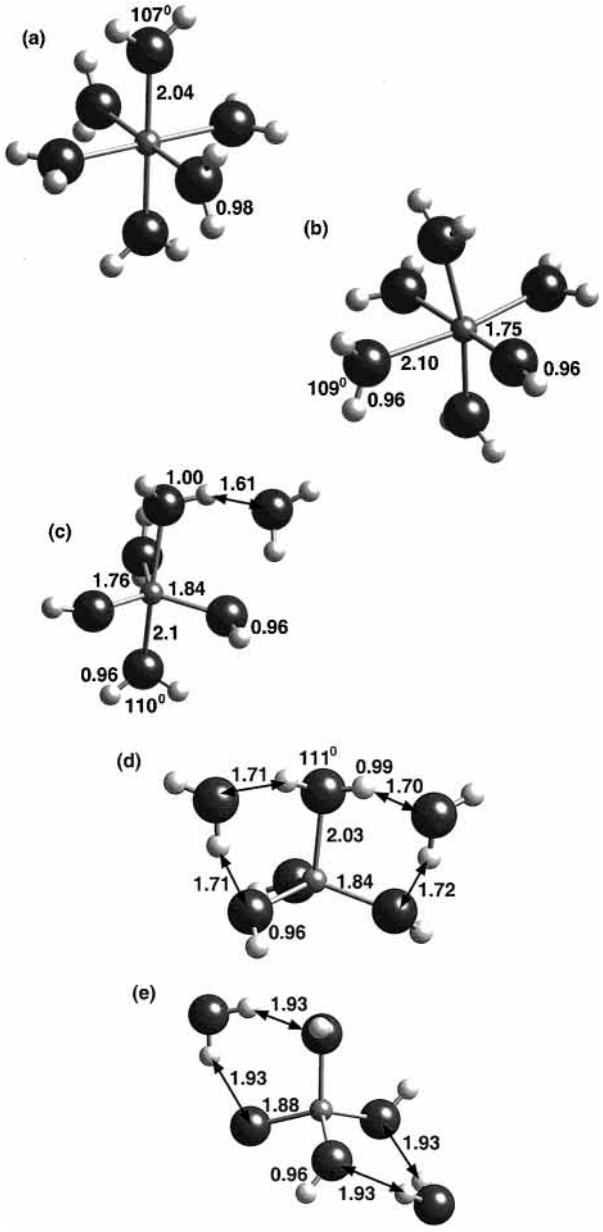

Figure 3. Species in the Fe^{3+} hydrolysis series: (a) [Fe^{3+}·6(H_2O)], (b) [$Fe(OH)^{2+}$·5(H_2O)], (c) [$Fe(OH)_2(H_2O)_3$]$^+$·(H_2O), (d) [$Fe(OH)_3$-(H_2O)]·2(H_2O) and (e) [$Fe(OH)_4$]$^-$·2(H_2O) as calculated with B3LYP/6-311G* in Gaussian 98.[11] The 6-fold to 5-fold coordination change predicted in the Al^{3+} model calculations also occurs in [$Fe(OH)_2(H_2O)_3$]·(H_2O) compared to the [$Al(OH)_3(H_2O)_2$]·(H_2O) species in Al^{3+} hydrolysis. Configurations in (c) and (d) were tested by adding extra water molecules of solvation.

species is predicted to be in tetrahedral coordination in contrast with the prediction of octahedral coordination based on hydrolysis data.[31] The hydrolysis species parallel the structures calculated for the Al^{3+} hydrolysis species, except that a pentacoordinate complex rather than an octahedral complex was predicted for [$Fe(OH)_2(H_2O)_3$]$^+$·(H_2O) (Figure 3c). Because the coordination changes predicted in the Al^{3+} hydrolysis series depended on the number of H_2O molecules used for solvation, additional water molecules were added to the [$Fe(OH)_2(H_2O)_3$]$^+$·(H_2O) and [$Fe(OH)_3(H_2O)$]·2(H_2O) complexes to test whether their structures would change with further solvation.

Ten water molecules were added to the [$Fe(OH)_2(H_2O)_3$]$^+$·(H_2O) complex (Figure 3c) to form a trans octahedral [$Fe(OH)_2$-(H_2O)$_4$]$^+$·10(H_2O) complex as an initial starting geometry (Figure 4a). This starting structure was chosen to test if a second

TABLE 1: Comparison of Model Fe^{3+} Hydrolysis Structures as Calculated with HF/3-21G(d,p) and B3LYP/6-311G(d) Methods

complex	parameter	HF/3-21G(d,p)	B3LYP/6-311G(d)
$Fe^{3+}\cdot 6(H_2O)$	Fe−O	2.03	2.04
	O−H[1]	0.95	0.97
	HOH	106	106
$[Fe(OH)\cdot 5(H_2O)]^{2+}$	Fe−OH_2	2.07	2.11
	Fe−OH	1.74	1.75
	O−H[1]	0.95	0.97
	O−H[2]	0.93	0.96
	HOH	110	109
$[Fe(OH)_2\cdot 4(H_2O)]^{+}$	Fe−OH_2	2.07	2.11[3]
	Fe−OH	1.84	1.80
	O−H[1]	0.94	0.96
	O−H[2]	0.93	0.96
	HOH	114	110
$[Fe(OH)_3\cdot 3(H_2O)]$	Fe−OH_2	1.99[4]	2.02[4]
	Fe−OH	1.81	1.83
	O−H[1]	0.97	0.99
	O−H[2]	0.94	0.96
	HOH	115	111
$[Fe(OH)_4\cdot 2(H_2O)]^{-}$	Fe−OH	1.86[4]	1.88[4]
	O−H[2]	0.94	0.96

[a] 1 = H_2O, 2 = OH^-, 3 = pentacoordinate, Fe 4 = tetrahedral Fe.

solvation sphere would stabilize an octahedral configuration for $[Fe(OH)_2]^+$ over the pentacoordinate structure predicted for the small cluster. Indeed, a stable minimum was predicted for the octahedral configuration in this case. Martin et al.[2] performed similar calculations of Fe^{3+} hydrolysis and predicted energy differences on the order of 8 kJ/mol between the trans, cis and pentacoordinate species. Such small energy differences could be important because the conversion between a 6-fold and 5-fold coordinate species may play a role in the mechanism of ligand exchange.[2]

Energy minimizations of the cis (Figure 4b) and pentacoordinate (Figure 4c) $Fe(OH)_2^+$ complexes with the extra 10 water molecules resulted in a stable structure for the former and conversion to the trans octahedral configuration (Figures 4c and 4d) for the latter. The calculated potential energy of the *cis*-$[Fe(OH)_2(H_2O)_4]^+$ was −20 kJ/mol lower than that for the new trans configuration of this complex (not including an IEFPCM term because the clusters were too large to obtain a converged solution for the electron density within the dielectric continuum). One should also note that this second trans configuration was −10 kJ/mol lower than the previous energy-minimized trans configuration of the same species. This result points to a common problem with energy minimizations, namely, that more complex systems are more likely to lead to local minima on the potential energy surface that are not the lowest energy state (i.e., global minimum). Consequently, one must consider uncertainties on the order of 10 kJ/mol when interpreting the energies of these types of model calculations.

As was the case for the $Al(OH)_3$ complex, tetrahedral coordination was predicted for $Fe(OH)_3$ in a cluster with three additional water molecules. The explicit hydration of $[Fe(OH)_3(H_2O)]\cdot 2(H_2O)$ (Figure 3d) was increased by adding six water molecules to form $[Fe(OH)_3(H_2O)_2]\cdot 8(H_2O)$ (Figure 4e). As was predicted for the Al^{3+} hydrolysis, $Fe(OH)_3$ resulted in a pentacoordinate (trigonal bipyramidal) configuration when additional water molecules were present. Apparently, the energy gained by solvating the $[Fe(OH)_3(H_2O)]$ complex with two water molecules (Figure 3d) is greater than that lost by breaking the second Fe^{3+}-OH_2 bond in $[Fe(OH)_3(H_2O)_2]$. Four moderately strong H-bonds form in $[Fe(OH)_3(H_2O)]\cdot 2(H_2O)$ as evidence of this conclusion. In aqueous solution, the pentacoordinate configuration (Figure 4e) should be more stable because the

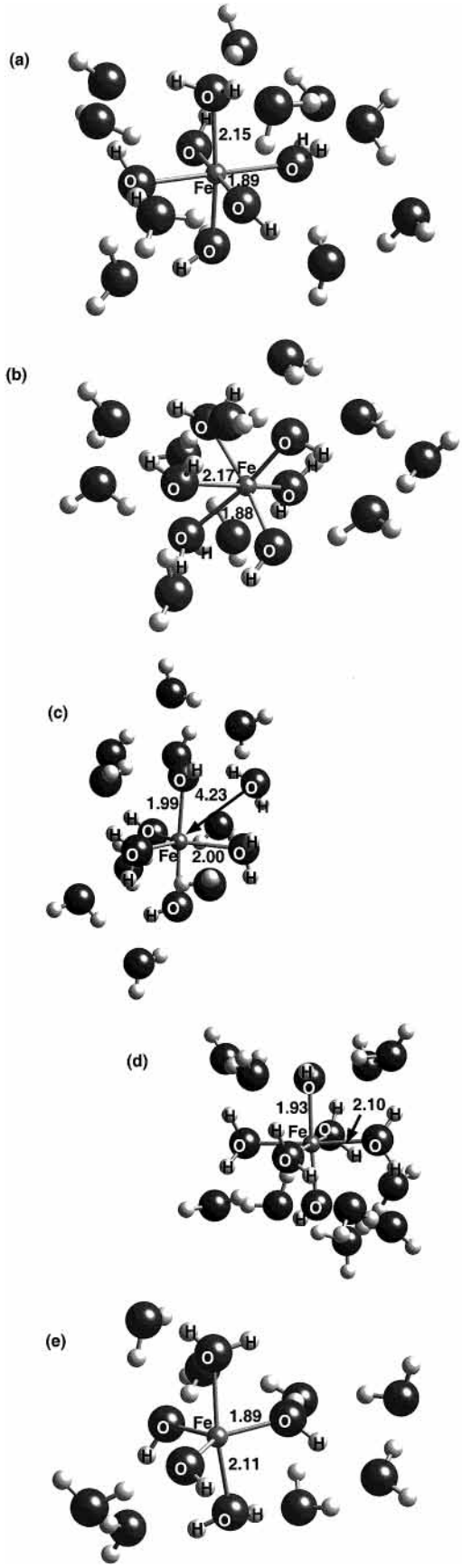

Figure 4. Species in the Fe^{3+} hydrolysis series (a) *trans*-$[Fe(OH)_2(H_2O)_4]^+\cdot 10(H_2O)$, (b) *cis*-$[Fe(OH)_2(H_2O)_4]^+\cdot 10(H_2O)$ are dynamically stable. (c) The 5-fold coordinate species, $[Fe(OH)_2(H_2O)_3]^+\cdot 11(H_2O)$, converts to the (d) 6-fold coordinate species, *trans*-$[Fe(OH)_2(H_2O)_4]^+\cdot 10(H_2O)$, during energy minimization. (e) Five-fold coordinate aqueous Fe^{3+} model of $[Fe(OH)_3(H_2O)_2]\cdot 8(H_2O)$.

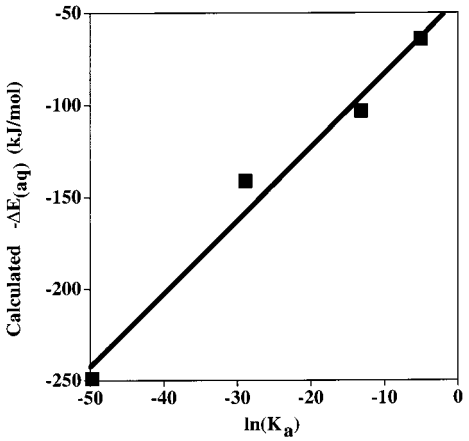

Figure 5. Calculated Fe^{3+} hydrolysis deprotonation energies plotted against experimental ln(K_a) (ref 32).

number of H_2O molecules is not limited as in these cluster calculations.

The lowest energy configurations in Figures 3 and 4 (minus any extra H_2O molecules of solvation) were used to calculate the molecular energies for Fe^{3+} hydrolysis aqueous solution with B3LYP/6-311G(d) basis sets and IEFPCM.[18] The correlation between theoretical energy changes in aqueous solution and the experimental ln(K_a)[32] is close to linear (Figure 5). In this case, however, the model temperature has a larger error. The slope in Figure 5 corresponds to a theoretical temperature of 481 K, about 180 K higher than expected. However, the model ΔS is approximately 88 J/mol-K, close to the ΔS found for deprotonation reactions.[28] The discrepancy in temperature could be due to a combination of four factors: the computational method for obtaining the aqueous energy is inadequate (e.g., basis set limitations or insufficient explicit hydration), model structures do not accurately reflect the aqueous Fe^{3+} species, Fe^{3+}-complexes may form in solution, or uncertainties in the K_as for aqueous Fe^{3+}. Using the other monomer configurations generated for species in the Fe^{3+} hydrolysis series will not reduce the calculated temperature error because alternative species are all higher in energy and would lead to a steeper slope and higher temperature estimate.

Si^{4+} Hydrolysis. All Si^{4+} species in this study were modeled with nine water molecules of solvation. The SCIPCM[13] was used for Si^{4+} due to this large solvation shell. The SCIPCM handles these large supermolecules more readily than IEFPCM because the solute cavity is based on an electron density cutoff (0.001 e^- in this case) rather than contact radii between solvent and solute. More extensive explicit solvation was useful in this case for two reasons. First, the Si^{4+} hydrolysis reactions of interest are from $[Si(OH)_3(OH_2)]^+$ to $[SiO_2(OH)_2]^{2-}$; therefore, hydroxyls and oxygen atoms rather than water molecules dominate the inner coordination sphere of the cation. Oxygen atoms in $Si-O^-$ bonds may be especially strong H-bond donor groups,[33] so inclusion of a full solvation sphere could be critical for obtaining accurate results. This condition is a departure from the Al^{3+} and Fe^{3+} cations that start out surrounded only by water molecules. Second, only two pK_a values are available for the Si^{4+} hydrolysis series. Results from these calculations will be used to predict a third pK_a for the reaction $[Si(OH)_3(OH_2)]^+ \rightarrow Si(OH)_4 + H^+$, requiring that the results of the other two deprotonation reactions be as accurate as possible. Inclusion of a larger solvation sphere can significantly improve model results with respect to pK_as.[17]

Model configurations calculated in this study are shown in Figure 6. H-bonding between orthosilicic acid, $Si(OH)_4$, and

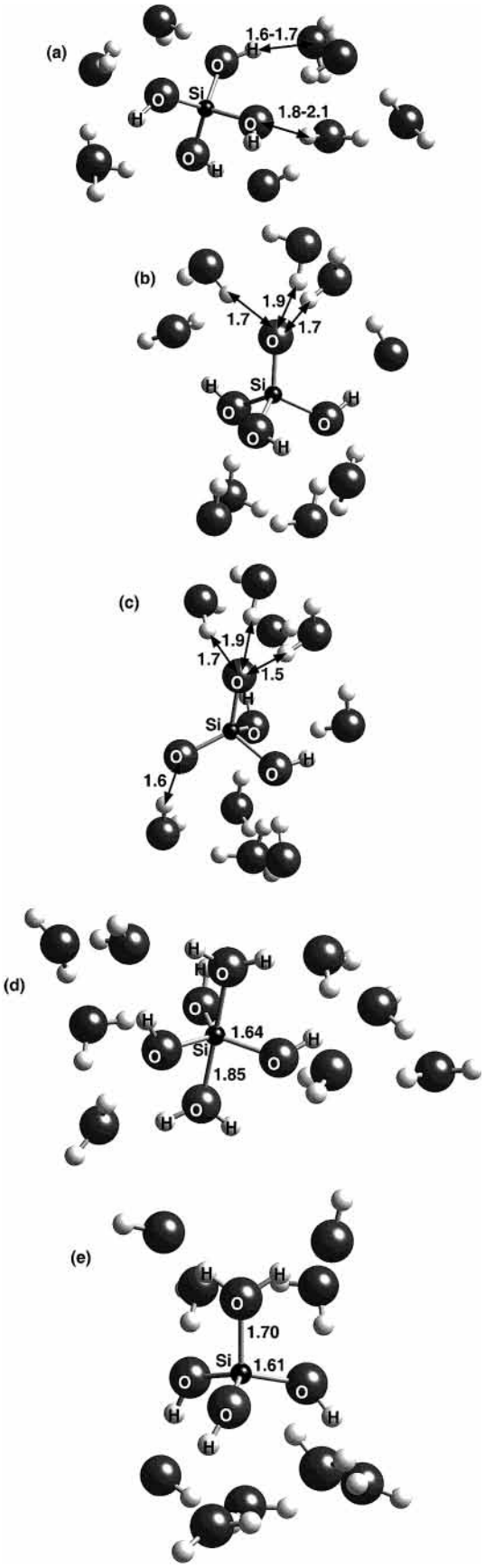

Figure 6. Model aqueous silica species: (a) $Si(OH)_4 \cdot 9(H_2O)$, (b) $[SiO(OH)_3]^- \cdot 9(H_2O)$, (c) $[SiO_2(OH)_2]^{2-} \cdot 9(H_2O)$, (d) 5-fold $[Si(OH)_3(H_2O)_2]^+ \cdot 8(H_2O)$, and (e) 4-fold $[Si(OH)_3(H_2O)]^+ \cdot 9(H_2O)$. Note the ability of the oxygen in the deprotonated SiO^- groups in (b) and (c) to form three H-bonds. This indicates that the $[SiO_2(OH)_2]^{2-} \cdot 9(H_2O)$ model is not fully hydrated in these calculations.

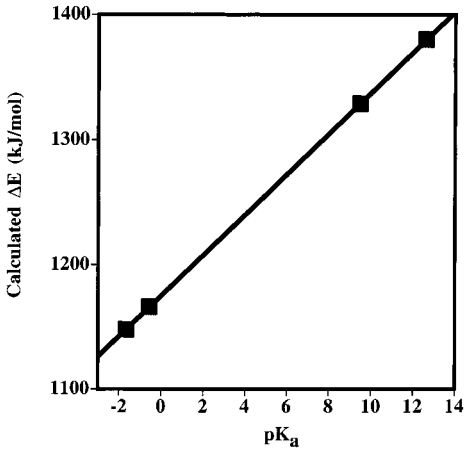

Figure 7. Calculated energy differences from $Si(OH)_4$ plotted against experimental pK_as (ref 36). The two points below pK_a = 0 are from Figure 6d and 6e with the pK_a values extrapolated from the two experimental points at pK_a = 9.47 and 12.60.

water occurs at almost every O and H atom in the four hydroxyls of this molecule. Average H-bond lengths are somewhat shorter (1.6 to 1.7 Å vs 1.8 to 2.1 Å; Figure 6a) when the water is the acceptor rather than the donor, which is indicative of stronger H-bonding. Pelmenschikov et al.[34] obtained similar results for calculations involving one water molecule H-bonding to orthosilicic acid.

Deprotonation of orthosilicic acid to form $[SiO(OH)_3]^-$ significantly changes the calculated solvation structure. As Rustad and Hay[33] predicted in molecular dynamics simulations using parameterized potentials, SiO^- groups have the potential to form three moderately strong H-bonds to water molecules (Figure 6b and 6c). This is the main reason the number of H_2O molecules in the model has been increased over the four that were used in Tossell and Sahai,[35] but even $Si(OH)_4$ should require 8 H_2O molecules to form a complete solvation sphere.

A plot of $-\Delta E_{(aq)}$ vs ln(K_a), similar to Figures 2 and 5, may not be meaningful in this case because there are only two known pK_as ($Si(OH)_4 \rightarrow [SiO(OH)_3]^-$, p$K_a$ = 9.47 and $[SiO(OH)_3]^- \rightarrow [SiO_2(OH)_2]^{2-}$, p$K_a$ = 12.60[36]); a correlation between two points will always be a line by definition. The change in energy between each species can be plotted against pK_a, however, as was done in Rustad et al.[37] to predict at which pH a third deprotonation reaction should occur. Figure 7 shows the calculated energy differences for the above two deprotonation reactions. Extrapolated from these two points, the calculated energy differences for the pentacoordinate $[Si(OH)_3(OH_2)]^+ \cdot 9(H_2O)$ (Figure 6d) and tetrahedral $[Si(OH)_3(H_2O)_2]^+ \cdot 8(H_2O)$ (Figure 6e) species are plotted. Using these values, a pK_a of approximately −2 is predicted for the reaction $[Si(OH)_3(H_2O)]^+ \rightarrow Si(OH)_4 + H^+$. This value is close to a proposed value for this reaction on silica gel.[38] Although the pK_a of surface silica species and aqueous species are not expected to be equal, they should fall within the same general range.[39] Prediction of a stable $[Si(OH)_3(OH_2)]^+$ species is important because it demonstrates the possibility of forming this species on silicate surfaces under low pH conditions. Common models of silicate surfaces assume this species,[39] but recent molecular modeling work has cast doubt on the stability of a $\equiv Si-(OH_2)^+$ type functional group in aqueous silica or on silicate surfaces.[37]

Conclusions

The main question regarding modeling methodology answered by this work is that explicit hydration of aqueous species must be included in order to generate a structure that resembles the dissolved cations. This is clear from the Al^{3+} and Fe^{3+} hydrolysis series that have different structures and coordination states for certain species depending on the number of water molecules included in the energy minimization. Hence, gas-phase calculations of proton affinities may not reflect aqueous-phase deprotonation reactions if the gas-phase species involves direct bonding to an H_2O molecule.

Second, the results presented here indicate that reasonable thermodynamic parameters of aqueous species may be calculated if the model is realistic and tested against experimental data. Correlations of deprotonation energy and pK_as, or similar variables, should rest on thermodynamic grounds [i.e., eqs 1−3] because energy differences can correlate with pK_as without any thermodynamic meaning. For example, earlier gas-phase calculations have been correlated with ln(K_a) for Al^{3+} hydrolysis, but the temperatures derived from this correlation can be as high as 1000 K.

Finally, the prediction of a stable $\equiv Si-(OH_2)^+$ at pH ≈ −2 is useful as research begins to reexamine some of the common assumptions regarding charging on silicate surfaces. Although this low pH is not encountered commonly in nature, the specific species controlling surface charges on silicate minerals is critical for understanding dissolution and adsorption reactions. $\equiv Si-(OH_2)^+$ may be stable under less acidic conditions depending on mineral type and may occur under natural conditions.

Acknowledgment. The author appreciates the time and effort put into the review process by two anonymous reviewers. J.D.K. acknowledges the financial support of the Office of Naval Research. Computational resources were also provided by the DoD High Performance Computing Initiative through the Aeronautical Systems Center (Dayton, OH) and the Space and Naval Warfare Systems Center (San Diego, CA).

References and Notes

(1) Dapprich, S.; Komaromi, I.; Byun, K. S.; Morokuma, K.; Frisch, M. J. *J. Mol. Str. (THEOCHEM)*, **1999**, *461*−*462*, 1.

(2) Martin, R. L.; Hay, P. J.; Pratt, L. R. *J. Phys. Chem. A* **1998**, *102*, 3565.

(3) Rustad, J. R.; Wasserman, E.; Felmy, A. R. *Surf. Sci.* **1999**, *424*, 28.

(4) Bakker, A.; Hermansson, K.; Lindgren, J.; Probst, M. M.; Bopp, P. A. *Int. J. Quantum Chem.* **1999**, *75*, 659.

(5) Lauenstein, A.; Hermansson, K.; Lindgren, J.; Probst, M.; Bopp, P. A. *Int. J. Quantum Chem.* **2000**, *80*, 892.

(6) Morel, F. M. M.; Hering, J. G. *Principles and Applications in Aquatic Geochemistry*; Wiley-Interscience: New York, 1993; 588 pp.

(7) Van Cappellen, P. *Chem. Geol.* **1996**, *132*, 125.

(8) Ainsworth, C. C.; Friedrich, D. M.; Gassman, P. L.; Wang, Z.; Joly, A. G. *Geochim. Cosmochim. Acta*, **1998**, *62*, 595.

(9) Binkley, J. S.; Pople, J. A.; Hehre, W. J. *J. Am. Chem. Soc.* **1980**, *102*, 939.

(10) Gordon, M. S.; Binkley, S.; Pople, J. A.; Pietro, W. J.; Hehre, W. J. *J. Am. Chem. Soc.* **1982**, *104*, 2797.

(11) Frisch, M. J.; Trucks, G. W.; Schlegel, H. B.; Scuseria, G. E.; Robb, M. A.; Cheeseman, J. R.; Zakrzewski, V. G.; Montgomery, J. A., Jr.; Stratmann, R. E.; Burant, J. C.; Dapprich, S.; Millam, J. M.; Daniels, A. D.; Kudin, K. N.; Strain, M. C.; Farkas, O.; Tomasi, J.; Barone, V.; Cossi, M.; Cammi, R.; Mennucci, B.; Pomelli, C.; Adamo, C.; Clifford, S.; Ochterski, J.; Petersson, G. A.; Ayala, P. Y.; Cui, Q.; Morokuma, K.; Malick, D. K.; Rabuck, A. D.; Raghavachari, K.; Foresman, J. B.; Cioslowski, J.; Ortiz, J. V.; Stefanov, B. B.; Liu, G.; Liashenko, A.; Piskorz, P.; Komaromi, I.; Gomperts, R.; Martin, R. L.; Fox, D. J.; Keith, T.; Al-Laham, M. A.; Peng, C. Y.; Nanayakkara, A.; Gonzalez, C.; Challacombe, M.; Gill, P. M. W.; Johnson, B. G.; Chen, W.; Wong, M. W.; Andres, J. L.; Head-Gordon, M.; Replogle, E. S.; Pople, J. A. *Gaussian 98*, revision A.7; Gaussian, Inc.: Pittsburgh, PA, 1998.

(12) Peng, C.; Ayala, P. Y.; Schlegel, H. B. *J. Comput. Chem.* **1996**, *17*, 49.

(13) Foresman. J. B.; Frisch, Æ. *Exploring Chemistry with Electronic Structure Methods: A Guide to Using Gaussian*, 2nd ed.; Gaussian Inc.: Pittsburgh, PA, **1996**, 269 pp.

(14) Pople, J. A.; Schlegel, H. B.; Krishnan, R.; Defrees, D. J.; Binkley, J. S.; Frisch, M. J.; Whiteside, R. A.; Hout, R. F.; Hehre, W. J. *Int. J. Quantum Chem.: Quantum Chem. Symp.* **1981**, *15*, 269.

(15) Becke, A. D. *J. Chem. Phys.* **1993**, *98*, 5648.

(16) Lee, C. T.; Yang, W. T.; Parr, R. G. *Phys Rev B*, **1988**, *37*, 785.

(17) Li, J.; Fisher, C. L.; Chen, J. L.; Bashford, D.; Noodleman, L. *Inorg. Chem.* **1996**, *35*, 4695.

(18) Cancès, E.; Mennucci, B.; Tomasi, J. *J. Chem. Phys*. **1997**, *107*, 3032.

(19) Keith, T. A.; Frisch, M. J. In *Modeling the Hydrogen Bond*, *ACS Symposium Series* 56; Smith, D. A., Ed.; ACS, Washington, DC, **1994**, 22.

(20) Kubicki, J. D.; Apitz, S. E.; Blake, G. A. *Geochim. Cosmochim. Acta*. **1996**, *60*, 4897.

(21) Kubicki, J. D.; Sykes, D.; Apitz, S. E. *J. Phys. Chem. A*, **1999**, *103*, 903.

(22) Marcus, Y. *Chem. Rev.* **1988**, *88*, 1475.

(23) Lubin, M. I.; Bylaska, E. J.; Weare. J. H. *Chem. Phys. Lett.* **2000**, *322*, 447.

(24) Phillips, B. L.; Tossell, J. A.; Casey, W. H. *Environ. Sci. Technol.* **1998**, *32*, 2865.

(25) Moolenaar, R. J.; Evans, J. C.; McKeever, L. D. *J. Phys. Chem*. **1970**, *74*, 3629.

(26) Rudolph, W. W.; Mason, R.; Pye, C. C. *Phys. Chem. Chem. Phys*. **2000**, *2*, 5030.

(27) Wesolowski, D. J.; Palmer, D. A. *Geochim. Cosmochim. Acta*, **1994**, *58*, 2947.

(28) Ridley, M. K.; Palmer, D. A.; Wesolowski, D. J.; Kettler, R. M. *Geochim. Cosmochim. Acta*, **1998**, *62*, 2279.

(29) Sykes, D.; Kubicki, J. D.; Farrar, T. C. *J. Phys. Chem.* **1997**, *101*, 2715.

(30) Ohtaki, H.; Radnai, T. 1993 *Chem. Rev.* **1993**, *93*, 1157.

(31) Martin, R. B. *J. Inorg. Biochem*. **1991**, *44*, 141.

(32) Langmuir, D. *Aqueous Environmental Geochemistry*; Prentice Hall Inc.: Upper Saddle River, NJ, 1997; p 349.

(33) Rustad, J. R.; Hay, B. P. *Geochim. Cosmochim. Acta* **1995**, *59*, 1251.

(34) Pelmenschikov, A. G.; Morosi, G.; Gamba, A. *J. Phys. Chem.* **1992**, *96*, 7422.

(35) Tossell, J. A.; Sahai, N. *Geochim. Cosmochim. Acta*, **2000**, *64*, 4097.

(36) Sjöberg, S.; Nordin, A.; Ingri, N. *Mar. Chem.* **1981**, *10*, 521.

(37) Rustad, J. R.; Wasserman, E.; Felmy, A. R.; Wilke, C. 1998 *J. Colloid Interface Sci.* **1998**, *198*, 119.

(38) Healy, T. W. *J. Macromol. Sci.-Chem.* **1974**, *A8*, 603.

(39) Schindler, P. W.; Stumm, W. In *Aquatic Surface Chemistry*, W. Stumm (ed.), John Wiley & Sons: New York, 1987; p 83.